Research Article | Vol. 30, No. 26 / 19 Dec 2022 / Optics Express 47612

Optics EXPRESS

High-speed tunable optical absorber based on a coupled photonic crystal slab and monolayer graphene structure

MINGSEN PAN,[1,3] AARON LIU,[1,2] ZHONGHE LIU,[1] AND WEIDONG ZHOU[1,*]

[1]Department of Electrical Engineering, University of Texas at Arlington, Arlington, Texas 76019, USA
[2]St. Mark's School of Texas, 10600 Preston Rd. Dallas, Texas 75230, USA
[3]mingsen.pan@uta.edu
[*]wzhou@uta.edu

Abstract: Reconfigurable metasurfaces have been pursued intensively in recent years for the ability to modulate the light after fabrication. However, the optical performances of these devices are limited by the efficiency, actuation response speed and mechanical control for reconfigurability. In this paper, we propose a fast tunable optical absorber based on the critical coupling of resonance mode to absorptive medium and the plasma dispersion effect of free carriers in semiconductor. The tunable absorber structure includes a single-layer or bi-layer silicon photonic crystal slab (PCS) to induce a high-Q optical resonance, a monolayer graphene as the absorption material, and bottom reflector to remove transmission. By modulating the refractive index of PCS via the plasma dispersion of the free carrier, the critical coupling condition is shifted in spectrum, and the device acquires tuning capability between perfect absorption and total reflection of the incident monochromatic light beam. Simulation results show that, with silicon index change of 0.015, the tunable absorption of light can achieve the reflection/absorption switching, and full range of reflection phase control is feasible in the over coupling region. The proposed reconfigurable structure has potential applications in remote sensing, free-space communications, LiDAR, and imaging.

1. Introduction

The ability to control and detect electromagnetic (EM) waves with reconfigurable optical component is important for optical sensing, communication, detection, and imaging. Chip-scale detection and manipulation of light is one of the most important challenges in the application of artificial materials, such as metamaterials and metasurfaces. By introducing an embedded layer of reconfigurable metasurfaces, the research on the optical sensing and communication have gained much progress in detecting and controlling EM waves and information simultaneously. As one of emerging remote sensing methods, light Detection and Ranging (LiDAR) systems employ the laser radiation energy, similar with the radar, for the detection of surrounding environment created both naturally and artificially [1]. An object or terminal with actively reconfigurable surface acquires the capability to modulate the incoming probing signals (optical beams) to achieve sensing and communications between the LiDAR sources. Similar technology includes the vehicle-to-vehicle (V2V) communications [2] and asymmetric free-space optical communications [3].

The LiDAR sensing platform usually uses high-power pulsed laser sources as the probing light to penetrate signals through the complex environment and media and compensate the scattering loss for detectable returned signals. On the one hand, the demonstration of high-power high-brightness and low-divergence lasers, such as the photonic crystal surface-emitting laser (PCSEL) provides practical solutions to the LiDAR sensing [4–6]. On the other hand, a non-dispersive

#476763 https://doi.org/10.1364/OE.476763
Journal © 2022 Received 28 Sep 2022; revised 29 Nov 2022; accepted 29 Nov 2022; published 14 Dec 2022

Optics EXPRESS

surface with reconfigurable response to the optical beams can serve as a multifunction terminal for the free-space optical communication, enabling multiple military and civilian applications with the free-space communication, for example, from Li-Fi to aircraft-satellite communications. Recently, a novel idea of reconfigurable intelligent surface (RIS) is proposed for the smart reconfiguration of wireless communication network [7]. As a new type of application similar to the metasurfaces concept, the RIS features reconfigurable optical links [8–10] for free-space optical communications. To adapt to the huge amount of detection and actuation operations in electro-optical signal coding/decoding and information processing, the response speed is one of the major challenges in the application.

The discovery of perfect optical absorber to plane waves [11] brings another significant dimension to the sensor performance, which suggests an EM wave is detected without reflecting any light back and secures the invisibility to the detection sources. In this regard, the modulation between total reflection and absorption can enhance the signal by reducing the background noise for free-space optical communication. The enhancement of optical absorption by metamaterials design has been reported on several platforms and structures, such as, plasmon nanoparticles [12]/nanoporous metal surface/localized surface plasmon resonance [13], critical coupling at resonance frequency with the MoS_2 monolayer [14]/graphene monolayer [15–18]. A single layer of graphene can implement perfect absorption with the plasmonic resonance effect of the polariton excitation by tailoring the graphene into ribbon [19], disk [20], nanowires [21]/gratings [22], or hybrid structures [23]. Although such plasmon-enhanced or plasmonic resonance-enhanced light-matter interaction can achieve perfect absorption, the metal loss in the optical spectrum range can significantly reduce the absorption tuning range and degrade the responsivity for some high-sensitive applications. By utilizing the switchable birefringence of refractive index of liquid crystal (LC) in the ordinary and extraordinary rays in the presence of an electric field, an electronically tunable absorber in the THz regime is realized. [24] However, these designs are limited by the tuning range of optical absorption and the modulation speed of liquid crystal is at MHz level and the efficiency and stability of LC-based modulator is relatively low.

In this paper, we investigate a high-speed optical tunable absorber based on a critically coupled photonic crystal slab (PCS) and graphene structure. The concept of critical coupling has been proposed and demonstrated experimentally with a passive structure built with the PCS and graphene monolayer [15,18]. The PCS is designed to be an optical filter which possesses a high-Q resonator with a small decay rate to match the graphene loss for critical coupling. The resonance frequency of the filter can be tuned by modulating the refractive index of PCS via the plasma dispersion of the free carrier [25]. Thus, in a critically coupled system, by controlling the resonant frequency, the monochromatic probing light beams can be either perfectly absorbed or reflected by the optical tunable absorber. We implement silicon refractive index modulation by the free carrier plasma dispersion effect [25–27]. Such designs are based on all solid materials, and it does not include any mechanical actuators. The response speed can reach 1 GHz for 20 μm devices [27]. The simulation results show the tunable device can switch its states between total absorption and reflection by the electro-optical modulation of the silicon PCS refractive index. Full range of reflection phase shift control can be achieved in the over coupling region. The proposed fast optical tunable absorber structures have potential application in the optical communication, LiDAR sensing, detection, and imaging.

2. Optical properties of critically coupled system

Photonic crystal slab (PCS) is a layer of thin compact two-dimensional (2D) photonic crystals etched into a slab of semiconductor. PCS can function as a quasi-3D structure where the in-plane guided resonance modes arise from the 2D photonic bandgap confinement and vertical light confinement from the material index difference [28,29]. The guided modes in the PCS appear as Fano resonances to the incoming electromagnetic waves, in which the optical properties can be

Optics EXPRESS

modelled by the temporal coupled mode theory [29–31]. When the leakage rate of one optical mode is equal to the material absorption rate contributed to the mode, critical coupling happens, and all the incident light will be absorbed. Even a single-layer graphene sheet placed near the mode can totally absorb the optical mode in the PCS under such critical coupling conditions [16,18].

The single-layer graphene introduces optical loss to the PCS guided mode as an intrinsic loss rate δ. Considering the lossless cavity decay rate γ_e for the PCS mode, the reflection coefficient can be derived as [15],

$$\Gamma(\omega) = \frac{j(\omega - \omega_0) + \delta - \gamma_e}{j(\omega - \omega_0) + \delta + \gamma_e} \tag{1}$$

where ω_0 is the resonant frequency of the PCS mode. It is obvious that, at the resonance frequency $\omega = \omega_0$, when $\delta = \gamma_e$, the reflection coefficient becomes $\Gamma(\omega_0) = 0$ and the system becomes reflectionless. Total absorption can be achieved by forcing the transmission to 0 by placing an optical reflector at the bottom. The absorptance thus is,

$$A(\omega) = 1 - |\Gamma(\omega)|^2 = \frac{4\delta\gamma_e}{(\omega - \omega_0)^2 + (\delta + \gamma_e)^2}. \tag{2}$$

When $\omega = \omega_0$, and $\delta = \gamma_e$, Eq. (2) becomes $A(\omega_0) = 1$. The phase of reflection can be calculated from the coefficient in Eq. (1) as

$$\varphi(\omega) = arctan\left(\frac{j(\omega - \omega_0) + \delta - \gamma_e}{j(\omega - \omega_0) + \delta + \gamma_e}\right) \tag{3}$$

where the arctan function calculates the angle of the complex S_{11} parameter. At different coupling conditions, we can obtain different range of reflection phase controls. At the critical coupling condition $\delta = \gamma_e$, the phase is $\varphi(\omega) = arctan(C + jD)$, in which $C = \frac{(\omega - \omega_0)^2}{(\omega - \omega_0)^2 + 4\delta^2}$ and $D = \frac{2\delta(\omega - \omega_0)}{(\omega - \omega_0)^2 + 4\delta^2}$. Due to the flip of sign in D when ω sweeps from $\omega < \omega_0$ to $\omega > \omega_0$, there is a π phase jump (i.e., phase singularity) at the resonant point.

To numerically calculate and analyze the absorption performance, we use a rigorous coupled wave analysis (RCWA) tool provided by Stanford S4 solver [32] to retrieve the complex S-parameters. The 2D periodic structure is modelled in one unit cell and the reflection/transmission/absorption spectra are calculated. Fig. 1 (a) shows a silicon PCS structure coupled with a graphene monolayer on a glass substrate. The PCS is an optical filter design with 2D circular air hole arranged in a square lattice with lattice constant a = 770 nm and slab thickness t = 249 nm. To design an optical filter and create a resonance near 1550 nm, the air hole shape is chosen to be circular, which has less scattering loss to the modes and thus possesses high Q factor. The square lattice introduces a 90-degree symmetry which has induced optical feedback in two directions for Q factor enhancement. The incident light beam, either Ex-polarized or Ey-polarized due to the 90-degree symmetry of the PCS lattice, is shone onto the structure from the normal direction. The monolayer graphene is prepared and attached to the top of the PCS layer directly with the polymethyl methacrylate (PMMA) transfer supporting layer with thickness of 180 nm. The graphene layer thickness is ~0.34 nm, and the complex refractive index is considered as n = 3.2584, k = 2.4222 at the design wavelength of 1550nm [33]. The refractive index is 1.45 for the glass, and 1.48 for the PMMA. Separated by a 1-μm silica spacer, 2.5 pairs of silicon/silica distributed Bragg reflectors (DBRs) are placed below the PCS to provide enhanced reflection and coupling for the incident light with the graphene loss near the center design wavelength 1550 nm. In such a one-port system, the transmittance is $T \approx 0$ due to the bottom reflector and the absorptance is A = 1 – R. At r = 76.9 nm, the absorptance is A = 1. This point is called critical coupling condition for total absorption of incoming light where no light gets reflected at the resonant wavelength.

Optics EXPRESS

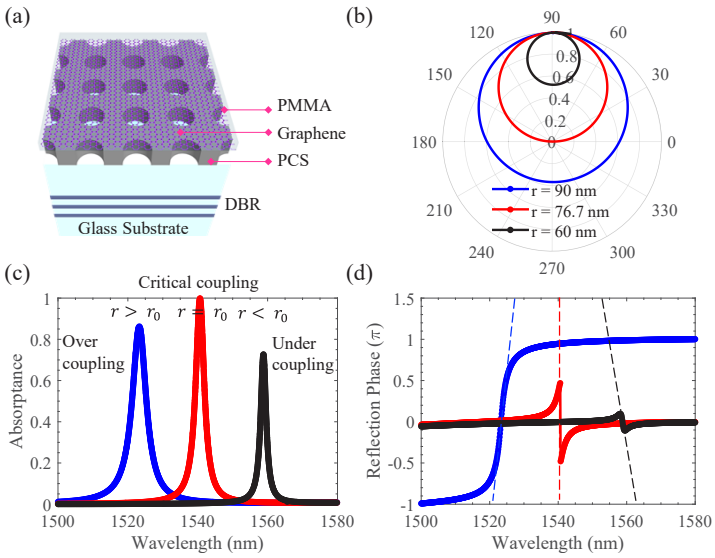

Fig. 1. Optical properties for a graphene monolayer and PCS coupled structure. (a) The structure includes 180 nm PMMA on top to bond a single layer of graphene on the PCS slab. The substrate has a two and a half periods of DBR 1 μm below the PCS layer separated by the silica spacer. The PC layer has a thickness of 249 nm and lattice constant 770 nm. (b) Polar plot of the S_{11} parameters with the radius of the air holes 90 nm (blue line), 76.7 nm (red line), and 60 nm (black line), respectively. (c)-(d) Absorptance (c) and reflection phase (d) of the three different coupling configurations. Perfect absorption happens at the critical coupling condition where $r = r_0$. The dashed lines in (d) are the gradient of phase change at the resonance locations.

Three cases are considered when the air hole radius is r = 60 nm, 76.9 nm, and 90 nm, corresponding to the under-coupling, critical coupling, and over-coupling conditions. The complex reflection coefficients of the incident light in the spectral range of 1500 nm to 1580 nm are shown in the polar plots in Fig. 1 (b) for the three cases. Fig. 1 (c) shows that the resonance wavelength for the three cases are 1563.11 nm, 1544.88 nm, and 1527.44 nm when the PCS air hole radius is r = 60 nm, 76.9 nm, and 90 nm, respectively. When changing to a larger radius, the circle of reflection in the polar plot becomes larger and passes 0 at 76.9 nm where the reflection is 0. The lossless cavity decay rate can be calculated from spectrum simulation results of the structure without the graphene layer. For the structure without graphene in Fig. 1 (a), the Q factors are 3064.5, 1029.5, and 501.98, and the cavity decay rates γ_e are 0.0313, 0.0942, and 0.1957 THz for r = 60 nm, 76.9 nm, and 90 nm, respectively. As shown in Fig. 1 (c)(d), the total absorption happens at 1540.64 nm where there is a π phase jump in the reflection phase. Coupled with the monolayer graphene, the PCS resonance modes acquire addition loss of δ and the total loss rates are $\delta + \gamma_e = 0.1166$, 0.1871, and 0.3058 THz for r = 60 nm, 76.9 nm, and 90 nm, respectively. At r = 76.9 nm, the decay rate from the lossless cavity is closed to the loss rate provided by the graphene, $\delta \approx \gamma_e$ and it shows near-perfect absorption due to the critical coupling. The dashed lines in Fig. 1 (d) are the reflection phase change gradient/sensitivity at the resonance location (i.e., the absorptance peak location) in these different coupling regions. Different phase tuning range for the reflected wave can be observed in these coupling regions. Full 2π reflection phase shift control (blue line) can be realized in the over-coupling region ($\delta < \gamma_e$). In the under-coupling region ($\delta > \gamma_e$), the phase shift is less than π (black line).

Optics EXPRESS

3. Optical phase sensing near critical coupling condition

The critical coupling condition induces a near perfect absorption at the resonance wavelength. Since the PCS guided resonance can be tuned by the material refractive index, one can expect the resonance detuning happens according to the refractive index change. Such light-matter interaction establishes a sensing protocol based on the resonance frequency shift and the refractive index change [34]. As shown in Fig. 2, the absorptance and reflectance shifts when the refractive index of silicon changes from 3.47 to 3.49. The importance is the critical coupling condition preserves for each working point, as the reflection phase has the phase singularities (π phase jump). By tracking the wavelength where maximum absorption happens, the refractive index information, which is influenced by the temperature, environment material, etc., can be retrieved. Fig. 2 shows the refractive index sensing scheme has sensitivity of ~4.24 nm per 0.01 refractive index unit (RIU).

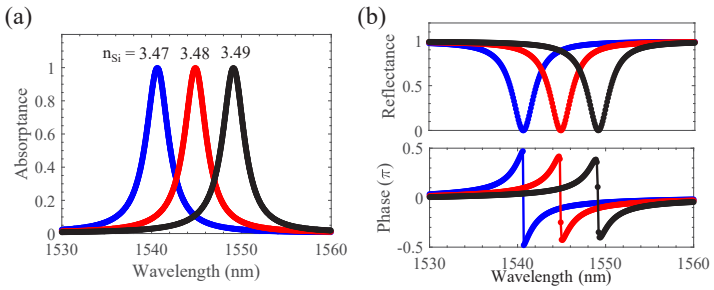

Fig. 2. Absorption/Reflection spectrum detuning induced by refractive index change. The structure is at the critical coupling condition mentioned in Fig. 1, and the air hole radius is 76.9 nm. (a) Absorptance spectra with silicon PCS refractive index 3.47 (blue), 3.48 (red), and 3.49 (black), respectively. (b) Reflectance (top panel) and reflection phase (bottom panel) spectra.

The sensitivity for the absorptance peak-tracking method can be further improved by the PCS design, such as the PCS mode volume and light confinement to enhance the mode overlap with the PCS material. It is worth noting that, without the graphene monolayer, the reflection phase shift is 2π for all three coupling conditions due to the large reflection coupling enhancement factor [35] induced by the bottom reflector. The single-layer graphene brings about the linewidth broadening effect which is not favorable for sensing. However, the abrupt phase gradient change in the reflection wave at the resonance frequency offers enhanced sensitivity.

Fig. 3 shows the conceptual scheme of phase sensing where the reflection phase change gradient flips sign at different coupling conditions. The sensitivity of the phase sensing scheme is calculated as slope of the reflection phase change at the resonance frequency (i.e., the absorption peak frequency) in the spectra, as shown in the dashed lines in Fig. 1 (d). At the critical coupling condition, as shown the red lines in Fig. 1 (d), the phase gradient becomes infinite at the phase singularity point. The over-coupling and under-coupling regimes give different sign of phase gradient, shown in Fig. 3 (a). The red and blue lines in Fig. 3 (a) track the change in the absorption peak and phase gradient, respectively, as the air hole radius changing from the over-coupling, critical coupling, to under-coupling regions. It is worth noting that the phase sensing scheme has higher sensitivity near the critical coupling position. Such enhanced sensitivity near the resonance location boosts further perturbation detection from thermally induced environment variables or liquid concentration, etc. at high speed.

The sensitivity for the absorption peak tracking method is,

$$S_A = \frac{\Delta\lambda}{\Delta n} \tag{4}$$

Optics EXPRESS

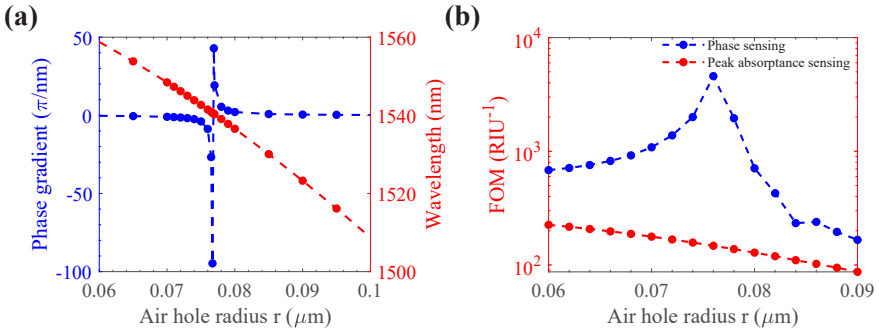

Fig. 3. Sensing scheme by reflection phase gradient. (a) Sensitivity of the phase gradient and resonance wavelength with different air hole radii. The phase gradient has enhanced sensitivity near the critical coupling condition. (b) FOM plots of the peak absorptance sensing and phase sensing schemes. Strong enhancement can be realized near the critical coupling condition (r = 76.9 nm).

and the FOM reads,

$$FOM_A = \frac{S_A}{\mathrm{d}\lambda} \tag{5}$$

where $\mathrm{d}\lambda$ is the full width at half maximum (FWHM) of the resonance lineshape. Similarly, to compare with the commonly used refractive index sensors that tracks the spectral shift of resonance in photonics, we introduce the figure of merit (FOM) [36] to the phase sensing scheme, and define the sensitivity for the reflection phase tracking method at the resonant wavelength as

$$S_{\varphi R} = \frac{\Delta \varphi R}{\Delta n} \tag{6}$$

and the FOM reads,

$$FOM_{\varphi R} = \frac{S_{\varphi R}}{\mathrm{d}\varphi R} \tag{7}$$

where $\mathrm{d}\varphi R$ is the reflection phase change within the FWHM of the reflection spectrum. We calculate the FOMs by introducing a perturbation to the refractive index of PCS layer in the simulation to shift the spectra within the FWHM. With the simulated index-absorption or index-phase data, the sensitives are calculated at the resonant wavelength according to Eq. (4) and Eq. (6), respectively. Then the FOMs are calculated with the sensitivity divided by the FWHM or the phase change within the FWHM. Fig. 3 (b) shows the higher $FOM_{\varphi R}$ (blue dashed line) for the phase sensing scheme than the FOM_A (red dashed line) for the resonance-tracking method. There exist enhancements of FOM with the phase sensing scheme near the critical coupling condition (i.e., r = 76.9 nm).

4. High-speed optical absorption/reflection modulation

Optical sensors and detectors with tunable optical properties provide faster data collection and powerful sensing capabilities to acquire the environmental variables. Thanks to the above-light-line nature of the guided resonance in a PCS, the optical modes are ideal candidates for the detection and formation of planar wavefronts for long-range free-space optical communication and information processing. On the other hand, the tunable optical absorber can be scaled into larger-area arrays to implement RIS functionality for spatial signal multiplexing, beam formation, communication relay, etc.

To implement a fast tunable optical absorber on the silicon photonics platform, we propose two electrically modulated structures based on the free carrier plasma dispersion effect [26,27,25], as

Optics EXPRESS

shown in Fig. 4. The basic structure for electro-optical modulation is a heterostructure with one or more P-Oxide-N or P-Intrinsic-N doping profiles. The oxide or the intrinsic layer functions as an electrical insulation between the P-doped and N-doped semiconductors, and the device can work as a parallel-plate capacitor to perform charging and discharging at high speed. The thickness of the intrinsic layer can be designed according to the electrical tuning range and compliance voltage. With bias voltage applied between the P-doped and N-doped regions, the injection charge accumulates near the intrinsic layer and changes the refractive index profiles. The refractive index shift in the PCS structure changes the optical resonance frequency and creates a tunable optical absorber/reflector for monochromatic light beams. Therefore, a relation between the bias voltage and refractive index change can be retrieved and the electro-optical modulation can be implemented. For a typical device working at 1550 nm, the peak value of refractive index change can reach 0.01 to 0.02 with 5 V applied voltage [27]. Possible inhomogeneous doping profiles may impact formation of the P-I-N structure due to the non-uniform doping concentration. Since the refractive index modulations are strongest at the P-I or N-I interfaces, we can avoid such doping issues by creating a uniform intrinsic layer between the P-doped and N-doped regions for electrical isolation using the thermal deposition and transfer printing technologies. Here, we focus on the optical design and use a uniform refractive index change in the optical simulations.

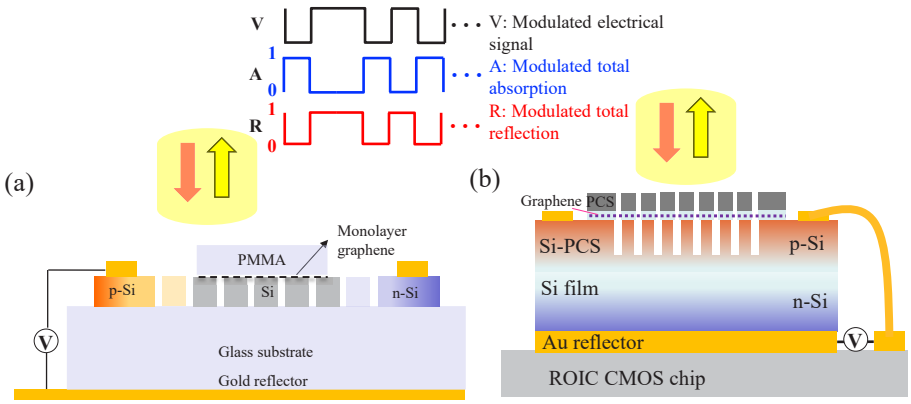

Fig. 4. Single-layer and double-layer PCS reflection/absorption modulator. (a) Horizontal doping of carriers across a single-layer PCS lattice region. The refractive index modulation of silicon PCS is realized by the in-plane carrier injection. (b) Vertical doping of carriers to modulate the bottom PCS refractive index of a double-layer PCS structure. The top layer PCS works as an optical filter for frequency selection and the bottom layer PCS functions as broadband reflector and index modulator. The color intensity marks the doping concentration.

By designing the pixel size of the single modulator device, optical response speed can reach 1 GHz on a 20 μm device [27]. One modulator design for the tunable optical absorber, shown in Fig. 4 (a), is implemented by a horizontal doping profile in the PCS plane. The PCS layer is fully etched through and the electrical carrier injection at the two electrodes placed at the p-Si and n-Si sides, respectively. The horizontal potential difference will excite the plasma effect near the PCS intrinsic Si region. The electro-optical properties can be fine-tuned to have better refractive index modulation efficiency. The other structure, shown in Fig. 4 (b), is double-layer PCS sandwiching a thin layer of silica spacer (10 nm to 20 nm thickness). The graphene monolayer is attached during the top-layer PCS processing. The top PCS layer is an optical filter for spectral selection and critical coupling with the graphene sheet. The bottom Si PCS serves as a broadband reflector for partially reflecting the incident wave for more efficiency lossless dielectric reflector. The electro-optical modulation is achieved in the thicker bottom-layer PCS silicon by vertical doping

Optics EXPRESS

gradient. Strong plasma effect is excited by the carrier injection and the refractive index change is transformed to the frequency detuning in the Fabry Perot (FP) cavity between the bottom gold reflector and the bottom PCS. As shown in the top inset of Fig. 4, by modulating the electrical bias voltage, the device can work to modulate and reflect the incident beam into digital signals for free-space optical communication.

The optical performances of the single-layer PCS coupled with monolayer graphene, shown schematically in Fig. 5 (a), are simulated with the RCWA method. Assuming refractive index of 3.48 for the Si PCS, Fig. 5 (b) depicts the Hz field amplitude distribution in one unitcell on the graphene layer plane and the cross-section plane in its left panel and right panel, respectively, at the excitation wavelength of 1548.39 nm with peak absorptance of 99.98%. The electric field directions of the excited mode, represented by the black arrows over the field profiles, are mainly oriented in parallel with graphene plane to sufficiently absorb the energy of the optical mode. The refractive index of gold reflector is taken as $n = 0.524 + 10.742i$ at center wavelength of 1550 nm. Simulation results of optical performances of the structure are shown in Fig. 5 (c)(d). The modulator design possesses near perfect absorption at the critical coupling condition, which can be tuned spectrally by modifying the PCS refractive index, shown in Fig. 5(c) and (d). The absorptance spectra show a slow varying envelop selected by the optical filter mode inside the PCS, and a fast oscillation due to the modulation of FP cavity formed in the thick glass substrate. The external cavity modulation can provide a much faster modulation of refractive index and absorption/reflection switching.

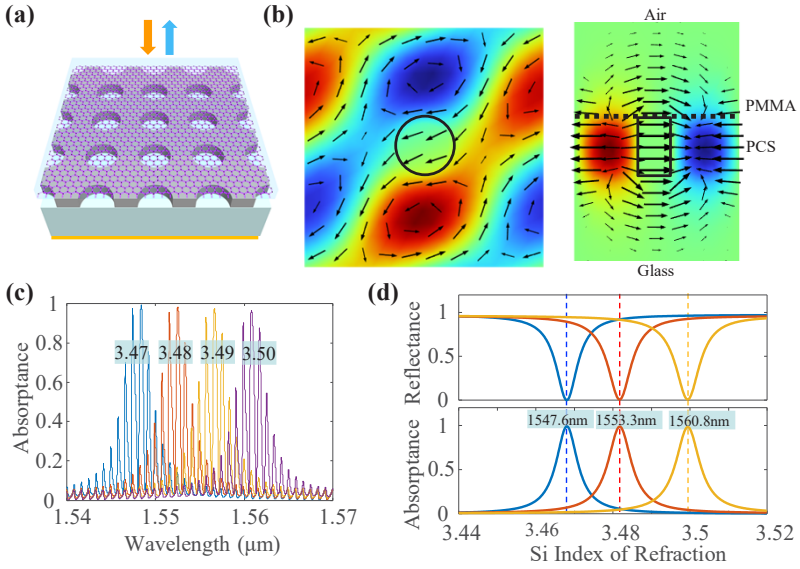

Fig. 5. Optical performance of the single-layer PCS modulator design. (a) Schematic of the graphene-PCS coupled structure. The graphene monolayer is transferred to a PCS layer (lattice design: a = 770 nm, r = 77 nm, t = 249 nm) by a thin layer of PMMA (180 nm). The substrate is 1 mm silica with back side deposited a gold mirror. (b) Simulated Hz field profiles in the graphene layer (left panel) and the cross section (right panel). The black arrows indicate the electric field direction. The circle and rectangular frames are the boundaries of the PCS air hole. The dashed line in the cross section is the graphene layer. (c) Absorptance spectrum of the structure with several difference Si indices from 3.47 to 3.50. (d) Absorptance and reflectance modulation by refractive index change of the silicon for three incoming monochromatic light at 1547.6 nm (blue), 1553.3 nm (red), and 1560.8 nm (yellow).

Optics EXPRESS

In the practical application, we define threshold values to determine the on and off states of the modulator. Fig. 6(a) shows an on-and-off optical switch whose on-state region is R > 90% and off-state region is R < 10%, marked by the red and blue shaded areas, respectively. To switch between the on and off operation states, the refractive index change for the single-layer PCS modulator design is $\Delta n_0 = \sim 0.015$, as shown in Fig. 6(a). The FOM of the modulator can be evaluated by calculating the extinction ratio (ER) between the operation states. Fig. 6 (b) shows the ERs for the single-layer and bi-layer PCS modulator designs, according to the equation, $ER(\Delta n) = 10\log\left(\frac{R(\Delta n)}{R_0}\right)$ where R_0 is the reflectance at the resonator frequency of the PCS mode. Here, the double-layer design, shown schematically in Fig. 4 (b), has top PCS layer with lattice constant 810 nm, thickness 230 nm, and air hole radius 60 nm, and bottom PCS layer with lattice constant 810 nm, etching depth 230 nm, and air hole radius 240 nm. The bottom PC is patterned on a Si film whose thickness is 10 µm. The two PC layers are separated by a 20 nm SiO_2 thin layer to separate the impact of the electrical injection on the optical filter in the top layer. The bi-layer PCS design requires silicon index change of ~0.005 with an extinction ratio of 20 dB for switching between reflection and absorption, which is much more efficient and sensitive compared to the single-layer design.

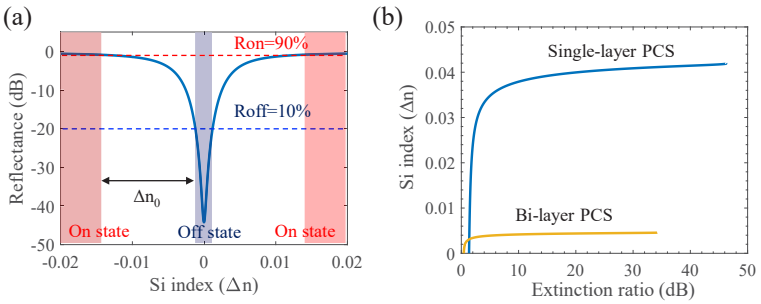

Fig. 6. Switching sensitivity plot of the single-layer and bi-layer PCS modulator designs. (a) Definition of on and off state for the optical switch with threshold value R = 0.9 and 0.1, respectively. The reflection curve is for the single layer PCS design. (b) Extinction ratio in dB as figure-of-merit plots for on and off states modulated by the silicon refractive index.

5. Discussions

5.1. Reflection phase control and sensing

In this paper, we explored the phase shift control on the proposed optical absorptance structure based on the coupling condition of graphene and resonance in the PCS. Near 2π phase control in the reflection can be achieved with over-coupling conditions. A phasing scheme is studied for refractive index sensing and enhanced sensitivity and FOM can be implemented near the critical coupling condition. As shown in Fig. 3 (b), The simulated sensor FOM of the absorption peak tracking method is 225.4 for the structure with air hole radius r = 60 nm, and 87 for r = 90 nm. Such FOM is comparable to the achievements in the current sensor technologies [36]. The corresponding phase sensing FOM is 683.1 when r = 60, and 166.3 for r = 90 nm. Near the critical coupling region, the phase sensing FOM is enhanced due to the more abrupt phase change brought by the enhanced absorption, and the FOM can reach above 4000. Therefore, the phase sensing method can improve the FOM and sensitivity of the current refractive index sensors. In this paper, we theoretically investigate the phase shift control of critically coupled structures and simulate the enhanced sensitivity. The results will bring interesting functionalities and improved performances to the sensor technologies in our future study.

Optics EXPRESS

5.2. Tunable optical absorbers

According to the actuation position, the tunable absorbers can be divided into two categories, one is the refractive index modulator, the other is the graphene modulator. There are several methods to modulate the refractive index, such as thermo-optical effect, liquid crystal, the Pockels effect, and the free carrier plasma dispersion. By tuning the Si index of photonic crystal with integrated microheaters, the frequency shift of a defect cavity resonant mode in an over 10 nm spectral tuning range is observed with switching speed of 10 kHz. [37] Another research investigated the graphene microheaters design and slow light supported by the photonic crystal waveguides, the thermo-optical response time for silicon photonics is reduced to 525 ns under 100 kHz driving sources [38].

The tunable optical absorber technologies are summarized in Table 1. Absorbing materials in the near-infrared (NIR) spectrum like metal films is not easy to implement full range absorption tuning. Tunability is limited by the predesigned metasurafce in the enhanced absorption by the localized surface plasmon resonance (LSPR), which has a low Q and broadband width [13]. Compared to meta-based surface plasmon polaritons (SPPs) absorption, graphene can introduce tunability to the absorption by tuning the Fermi energy of graphene [22,39]. Tunable absorptance of incident light was achieved in the range 45% to near 100% [39]. Such tuning method can reach a speed of around 1 GHz for devices with 25 μm size [40]. Full range of absorption tuning is challenging but possible in theory by applying a large enough voltage to move the Fermi energy of graphene and change the complex permittivity and the critical coupling condition. However, the optical modes in a ring resonator serve better for on-chip applications. In the free space, the modes will see large divergence compared to PCS guided resonant modes at the Γ point proposed in this paper. Liquid crystal (LC) is widely used technology in spatial light modulator (SLM), etc. By tuning the optical properties of metamaterials, it is feasible to implement a

Table 1. Comparisons of tunable optical absorbers

Platform	Absorber structure / Tuning mechanism	Tunable range/ speed	λ/Q	Voltage	Ref.
Gold/glass	Enhanced LSPR on nanoparticle metasurface / Predesigned/Not actively tunable	N.A.	1600 nm/ ~50	N.A.	[13]
Graphene/ dielectric	Enhanced excitation on metallic surface / Tuning SPPs on graphene	N.A.	23.57 μm/ N.A.	~4 V	[22]
LC/ metamaterial	Liquid crystal/ metamaterial / Metamaterial absorption	10% to 30%/ 1kHz to 100 kHz	2.62 (THz)/ N.A.	4 V	[24]
Silicon/ graphene	Graphene optical modulator / Fermi energy of graphene	~ 45% to 90%/ around 1 GHz	1300 nm/ 2600	4 V [40]	[39]
$LiNbO_3$/ graphene	Critically coupled LN and metamaterial / Resonance tuning, Pockels effect	Near full range/ MHz to over 1 GHz	798.42 nm/~800	300 V	[41]
Semiconductor/ graphene	Critically coupled PCS and graphene PCS resonance tuning; / Semiconductor plasmon dispersion	Near full range/ 200 MHz to over 1 GHz	1545 nm/~520	10 V [27]	This work

Optics EXPRESS

tunable optical absorber. In THz spectrum, a LC-based tunable modulator is designed which achieves 1kHz to 100 kHz speed with tunable range 30% to 10% [24]. Based on the Pockels effect in the electro-optic (EO) materials, such as the lithium niobate ($LiNbO_3$, LN), near full range of tunable optical absorber is achieved via the critical coupling of graphene to the LN material [41]. Similar with the absorption tuning mechanism proposed in this paper, the tunable absorber is built upon the critical coupling to the graphene to achieve complete absorption, and resonance tuning via the refractive index modulation. To achieve full range of absorption tuning, gate voltage from -150 V to 150 V is applied to introduce sufficient refractive index change. Such high voltage switching range may require special designs of the power sources and the device resistance/capacitance when operating at high speed. Based on the free carrier plasma dispersion effect in doped silicon, our proposed tunable optical absorber can achieve full range of absorption tuning at 200 MHz to over 1 GHz speed with 10 V bias voltage required.

5.3. Angle and polarization effect

In this paper, we designed PCS with a circular air hole arranged in square lattice to reduce the dependence on the polarization. The design of air hole shape and lattice has potential to more versatile application in tuning the absorption of light selectively in different polarization states.

The proposed PCS-graphene structure is designed for normal incidence, and the optical simulations assume isotropic medium for the monolayer graphene. For oblique incident light beams, high angular dispersion of Q factor of the PCS resonant modes may lead to the shift of critical coupling condition. Therefore, the polarization-dependence of optical absorption and reflection may be significant in the case of oblique incidence. The study of angular and polarization-dependent modal dispersion [42] can assist in understanding the interaction between oblique incident beams and the PCS-graphene coupled structure. Future study can extend the proposed concept of the PCS-based optical absorption tuning to arrays of modulators or sensors and to the tunable optical component for free-space optical communication with high responsivity to large incident angle.

6. Conclusion

In this paper, we explore the phase control and high-speed switch modulation of a tunable optical absorber based on critically coupled graphene-PCS structures. The critical coupling condition preserves when the PCS refractive index changes, which establish a phase sensing scheme for enhanced sensitivity near the resonance location. By modulating and harnessing the optical loss of a monolayer graphene at high speed, we investigate the high-speed optical reflection/absorption switching by modulating the refractive index of PCS and tuning the resonance wavelength. A more sensitive and efficient optical switching approach is proposed based on a bi-layer PCS structure. The simulation results show that an index change of 0.005 in silicon can switch the operation state of the device between near-perfect absorption and reflection with an extinction ratio of over 20 dB.

Disclosures. The authors declare no conflict of interest.

Data availability. Data underlying the results presented in this paper are not publicly available at this time but may be obtained from the authors upon reasonable request.

References

1. R. T. H. Collis, "Lidar," Appl. Opt. **9**(8), 1782–1788 (1970).
2. S. Eckelmann, T. Trautmann, H. Ußler, B. Reichelt, and O. Michler, "V2V-Communication, LiDAR System and Positioning Sensors for Future Fusion Algorithms in Connected Vehicles," Trans. Res. Procedia **27**, 69–76 (2017).
3. A. Maha, "Free-space optical communication by retromodulation: concept, technologies, and challenges," in *Proc.SPIE* (n.d.), 5614.
4. R. Sakata, K. Ishizaki, M. de Zoysa, S. Fukuhara, T. Inoue, Y. Tanaka, K. Iwata, R. Hatsuda, M. Yoshida, J. Gelleta, and S. Noda, "Dually modulated photonic crystals enabling high-power high-beam-quality two-dimensional beam scanning lasers," Nat. Commun. **11**(1), 3487 (2020).

Optics EXPRESS

5. A. Kalapala, A. Y. Song, M. Pan, C. Gautam, L. Overman, K. Reilly, T. J. Rotter, G. Balakrishnan, R. Gibson, R. Bedford, J. J. Coleman, S. Fan, and W. Zhou, "Scaling Challenges in High Power Photonic Crystal Surface-Emitting Lasers," IEEE J. Quantum Electron. **58**(4), 1–9 (2022).
6. S. Noda, K. Kitamura, T. Okino, D. Yasuda, and Y. Tanaka, "Photonic-Crystal Surface-Emitting Lasers: Review and Introduction of Modulated-Photonic Crystals," IEEE J. Sel. Top. Quantum Electron. **23**(6), 1–7 (2017).
7. M. A. ElMossallamy, H. L. Zhang, L. Y. Song, K. G. Seddik, Z. Han, and G. Y. Li, "Reconfigurable Intelligent Surfaces for Wireless Communications: Principles, Challenges, and Opportunities," IEEE Trans. Cogn. Commun. Netw. **6**(3), 990–1002 (2020).
8. H. Wang, Z. Zhang, B. Zhu, J. Dang, L. Wu, L. Wang, K. Zhang, Y. Zhang, and G. Y. Li, "Performance Analysis of Multi-Branch Reconfigurable Intelligent Surfaces-Assisted Optical Wireless Communication System in Environment With Obstacles," IEEE Trans. Veh. Technol. **70**(10), 9986–10001 (2021).
9. Z. Cao, X. Zhang, G. Osnabrugge, J. Li, I. M. Vellekoop, and A. M. J. Koonen, "Reconfigurable beam system for non-line-of-sight free-space optical communication," Light: Sci. Appl. **8**(1), 69 (2019).
10. 10. M. Najafi and R. Schober, "Intelligent Reflecting Surfaces for Free Space Optical Communications," in *2019 IEEE Global Communications Conference (GLOBECOM)* (n.d.), pp. 1–7.
11. D. Maystre and R. Petit, "Brewster incidence for metallic gratings," Opt. Commun. **17**(2), 196–200 (1976).
12. L. Zhou, Y. L. Tan, J. Y. Wang, W. C. Xu, Y. Yuan, W. S. Cai, S. N. Zhu, and J. Zhu, "3D self-assembly of aluminium nanoparticles for plasmon-enhanced solar desalination," Nat. Photonics **10**(6), 393–398 (2016).
13. N. Liu, M. Mesch, T. Weiss, M. Hentschel, and H. Giessen, "Infrared Perfect Absorber and Its Application As Plasmonic Sensor," Nano Lett. **10**(7), 2342–2348 (2010).
14. J. Wang, J. Z. Yang, and D. Shi, "Perfect absorption for monolayer transition-metal dichalcogenides by critical coupling," Nanotechnology **31**(46), 465205 (2020).
15. J. R. Piper and S. Fan, "Total Absorption in a Graphene Monolayer in the Optical Regime by Critical Coupling with a Photonic Crystal Guided Resonance," ACS Photonics **1**(4), 347–353 (2014).
16. J. R. Piper, V. Liu, and S. H. Fan, "Total absorption by degenerate critical coupling," Appl. Phys. Lett. **104**(25), 251110 (2014).
17. M. Zhang and X. Zhang, "Ultrasensitive optical absorption in graphene based on bound states in the continuum," Sci. Rep. **5**(1), 8266 (2015).
18. Y. H. Liu, A. Chadha, D. Y. Zhao, J. R. Piper, Y. C. Jia, Y. C. Shuai, L. Menon, H. J. Yang, Z. Q. Ma, S. H. Fan, F. N. Xia, and W. D. Zhou, "Approaching total absorption at near infrared in a large area monolayer graphene by critical coupling," Appl. Phys. Lett. **105**(18), 181105 (2014).
19. J. Christensen, A. Manjavacas, S. Thongrattanasiri, F. H. L. Koppens, and F. J. G. de Abajo, "Graphene plasmon waveguiding and hybridization in individual and paired nanoribbons," ACS Nano **6**(1), 431–440 (2012).
20. H. Yan, X. Li, B. Chandra, G. Tulevski, Y. Wu, M. Freitag, W. Zhu, P. Avouris, and F. Xia, "Tunable infrared plasmonic devices using graphene/insulator stacks," Nat. Nanotechnol. **7**(5), 330–334 (2012).
21. D. A. Kuzmin, I. v Bychkov, V. G. Shavrov, V. v Temnov, H. I. Lee, and J. Mok, "Plasmonically induced magnetic field in graphene-coated nanowires," Opt. Lett. **41**(2), 396–399 (2016).
22. S. X. Xia, X. Zhai, Y. Huang, J. Q. Liu, L. L. Wang, and S. C. Wen, "Multi-band perfect plasmonic absorptions using rectangular graphene gratings," Opt. Lett. **42**(15), 3052–3055 (2017).
23. A. Fallahi and J. Perruisseau-Carrier, "Design of tunable biperiodic graphene metasurfaces," Phys. Rev. B **86**(19), 195408 (2012).
24. D. Shrekenhamer, W.-C. Chen, and W. J. Padilla, "Liquid Crystal Tunable Metamaterial Absorber," Phys. Rev. Lett. **110**(17), 177403 (2013).
25. R. Soref and B. Bennett, "Electrooptical effects in silicon," IEEE J. Quantum Electron. **23**(1), 123–129 (1987).
26. D. Pérez-Galacho, D. Marris-Morini, R. Stoffer, E. Cassan, C. Baudot, T. Korthorst, F. Boeuf, and L. Vivien, "Simplified modeling and optimization of silicon modulators based on free-carrier plasma dispersion effect," Opt. Express **24**(23), 26332–26337 (2016).
27. Y.-C. Shuai, D. Zhao, Y. Liu, C. Stambaugh, J. Lawall, and W. Zhou, "Coupled Bilayer Photonic Crystal Slab Electro-Optic Spatial Light Modulators," IEEE Photonics J. **9**(2), 1–11 (2017).
28. W. Zhou, D. Zhao, Y.-C. Shuai, H. Yang, S. Chuwongin, A. Chadha, J.-H. Seo, K. X. Wang, V. Liu, Z. Ma, and S. Fan, "Progress in 2D photonic crystal Fano resonance photonics," Prog. Quantum Electron. **38**(1), 1–74 (2014).
29. S. H. Fan and J. D. Joannopoulos, "Analysis of guided resonances in photonic crystal slabs," Phys. Rev. B **65**(23), 235112 (2002).
30. D. A. Bykov and L. L. Doskolovich, "Spatiotemporal coupled-mode theory of guided-mode resonant gratings," Opt. Express **23**(15), 19234–19241 (2015).
31. S. H. Fan, W. Suh, and J. D. Joannopoulos, "Temporal coupled-mode theory for the Fano resonance in optical resonators," J. Opt. Soc. Am. A **20**(3), 569–572 (2003).
32. V. Liu and S. Fan, "S4: A free electromagnetic solver for layered periodic structures," Comput. Phys. Commun. **183**(10), 2233–2244 (2012).
33. B. K. Song, H. G. Gu, S. M. Zhu, H. Jiang, X. G. Chen, C. W. Zhang, and S. Y. Liu, "Broadband optical properties of graphene and HOPG investigated by spectroscopic Mueller matrix ellipsometry," Appl. Surf. Sci. **439**, 1079–1087 (2018).

Optics EXPRESS

34. Y. Liu, W. Zhou, and Y. Sun, "Optical Refractive Index Sensing Based on High-Q Bound States in the Continuum in Free-Space Coupled Photonic Crystal Slabs," Sensors **17**(8), 1861 (2017).
35. M. S. Pan, Z. H. Liu, A. R. K. Kalapala, Y. D. Chen, Y. Z. Sun, and W. D. Zhou, "Complete 2π phase control by photonic crystal slabs," Opt. Express **29**(25), 40795–40803 (2021).
36. R. Zafar and M. Salim, "Enhanced Figure of Merit in Fano Resonance-Based Plasmonic Refractive Index Sensor," IEEE Sens. J. **15**(11), 6313–6317 (2015).
37. Z. Xingyu, C. Swapnajit, C. Chi-Jui, P. Zeyu, Y. Hai, and T. C. Ray, "Microheater-integrated silicon coupled photonic crystal microcavities for low-power thermo-optic switching over a wide spectrum," in *Proc.SPIE* (n.d.), 9752.
38. S. Q. Yan, X. L. Zhu, L. H. Frandsen, S. S. Xiao, N. A. Mortensen, J. J. Dong, and Y. H. Ding, "Slow-light-enhanced energy efficiency for graphene microheaters on silicon photonic crystal waveguides," Nat. Commun. **8**(1), 14411 (2017).
39. X. Luo, Z. Liu, L. Wang, J. Liu, and Q. Lin, "Tunable ultra-narrowband and wide-angle graphene-based perfect absorber in the optical communication region," Appl. Phys. Express **11**(10), 105102 (2018).
40. M. Liu, X. Yin, E. Ulin-Avila, B. Geng, T. Zentgraf, L. Ju, F. Wang, and X. Zhang, "A graphene-based broadband optical modulator," Nature **474**(7349), 64–67 (2011).
41. X. Chen, Q. Meng, W. Xu, J. Zhang, Z. Zhu, and S. Qin, "Electrically tunable absorber based on a graphene integrated lithium niobate resonant metasurface," Opt. Express **29**(21), 32796–32803 (2021).
42. L. Chen, Z. Qiang, H. Yang, H. Pang, Z. Ma, and W. Zhou, "Polarization and angular dependent transmissions on transferred nanomembrane Fano filters," Opt. Express **17**(10), 8396–8406 (2009).